Seasonal and long-term consequences of esca on grapevine stem xylem integrity

Running title: Impact of the trunk disease esca on stem hydraulic integrity

Highlight: Our study reveals that esca can critically affect xylem water movement in grapevine perennial organs, by the presence of plant-derived tyloses.

G. Bortolami[a], E. Farolfi[a], E. Badel[b], R. Burlett[c], H. Cochard[b], N. Ferrer[a], A. King[d], L.J. Lamarque[c,e], P. Lecomte[a], M. Marchesseau-Marchal[a], J. Pouzoulet[f], J.M. Torres-Ruiz[b], S. Trueba[c,g], S. Delzon[c], G.A. Gambetta[f], C.E.L. Delmas[a*]

[a]INRAE, BSA, ISVV, SAVE, 33882 Villenave d'Ornon, France
[b]Université Clermont-Auvergne, INRAE, PIAF, 63000 Clermont-Ferrand, France
[c]Univ. Bordeaux, INRAE, BIOGECO, 33615 Pessac, France
[d]Synchrotron SOLEIL, L'Orme des Merisiers, Gif-sur-Yvette, 91192, France
[e]Département des Sciences de l'Environnement, Université du Québec à Trois-Rivières, Trois-Rivières, Québec, G9A 5H7, Canada
[f]EGFV, Bordeaux-Sciences Agro, INRAE, Université de Bordeaux, ISVV, 210 chemin de Leysotte, 33882 Villenave d'Ornon, France
[g]School of Forestry and Environmental Studies, Yale University, New Haven, CT 06511, USA

*Author for correspondence
Chloé E. L. DELMAS
chloe.delmas@inrae.fr
ORCID ID: 0000-0003-3568-605X

ABSTRACT

Hydraulic failure has been extensively studied during drought-induced plant dieback, but its role in plant-pathogen interactions is under debate. During esca, a grapevine (*Vitis vinifera*) disease, symptomatic leaves are prone to irreversible hydraulic dysfunctions but little is known about the hydraulic integrity of perennial organs over the short- and long-term. We investigated the effects of esca on stem hydraulic integrity in naturally infected plants within a single season and across season(s). We coupled direct (k_s) and indirect (k_{th}) hydraulic conductivity measurements, and tylose and vascular pathogen detection with in vivo X-ray microtomography visualizations. We found xylem occlusions (tyloses), and subsequent loss of stem k_s, in all of the shoots with severe symptoms (apoplexy) and in more than 60% of the shoots with moderate symptoms (tiger-stripe), and no tyloses in shoots that were currently asymptomatic. In vivo stem observations demonstrated that tyloses were observed only when leaf symptoms appeared, and resulted in more than 50% PLC in 40% of symptomatic stems, unrelated to symptom age. The impact of esca on xylem integrity was only seasonal and no long-term impact of disease history was recorded. Our study demonstrated how and to what extent a vascular disease such as esca, affecting xylem integrity, could amplify plant mortality by hydraulic failure.

Key words: Esca, hydraulic failure, plant dieback, tyloses, vascular pathogens, *Vitis vinifera* L., X-ray microCT, xylem anatomy

47 # INTRODUCTION

48 In agricultural and forest ecosystems, perennial plant dieback causes decreases in plant
49 productivity and longevity (Aleemullah and Walsh, 1996; Eskalen *et al*., 2013; Urbez-Torres
50 *et al*., 2013; Alvindia and Gallema, 2017). Plant dieback is a complex process where different
51 biotic and/or abiotic stress factors interact and contribute to leaf and crown wilting and
52 ultimately plant death (Desprez-Lostau *et al*., 2006; Anderegg *et al*., 2013, Cailleret *et al*.,
53 2017; Bettenfeld *et al*., 2020). Drought-mediated plant dieback has been extensively studied,
54 and in this case hydraulic failure has been identified as the primary cause of plant death
55 (Anderegg *et al*., 2016). Hydraulic failure results from an interruption of the ascendant water
56 flow by air embolism or xylem occlusion (Zimmermann, 1979; Tyree and Sperry, 1989).
57 Vascular pathogens, which infect the xylem network (Yadeta and Thomma, 2013), are also
58 important drivers of pathogen-mediated plant dieback (Goberville *et al.*, 2016; Pandey *et al*.,
59 2018; Fallon *et al*., 2020).

60 Vascular pathogens induce wood necrosis, leaf symptoms, and crown defoliation (Beckmann
61 and Roberts, 1995; Pearce, 1996). Their biology and toxic metabolite production has been well
62 studied, in particular using controlled phytotoxicity assays (Andolfi *et al.*, 2011; Akpaninyang
63 and Opara, 2017). However, the possible role of hydraulic failure during pathogen-mediated
64 plant dieback has been poorly investigated, and the underlying physiological mechanisms
65 inducing leaf symptoms are not clear yet (Fradin and Thomma, 2006; McDowell *et al*., 2008).
66 Moreover, the long-term impact (over seasons) and relationships between pathogens, leaf
67 symptom presence, and the hydraulic functioning of the plant are still unknown. During
68 vascular pathogenesis, both air (Pérez-Donoso *et al*., 2016) and nongaseous (Sun *et al*., 2013;
69 Czemmel *et al.,* 2015, Pouzoulet *et al*., 2019) embolism have been observed. For example, air
70 embolism is thought to accelerate pathogen progression during Pierce's disease (Pérez-Donoso
71 *et al*., 2016), and nongaseous embolism is associated with occlusion of the xylem conduits by
72 the plant that could slow the disease process while interfering with xylem water transport (Sun
73 *et al*., 2013; Pouzoulet *et al*., 2019).

74 Xylem occlusion, usually through the production of tyloses and gels, is one of the first plant
75 defense mechanisms against vascular pathogens (Pearce, 1996). Xylem parenchyma cells
76 secrete gels and expand into the vessel lumen, forming tyloses, physically blocking pathogen
77 progression (Zimmermann, 1979). Xylem anatomy plays an important role, both for vascular
78 pathogen development (Martin *et al*., 2009; Martín *et al*., 2013; Venturas *et al*., 2014;

Pouzoulet *et al*., 2017; 2020) and for tylose formation (Bonsen and Kucera, 1990; De Micco *et al*., 2016; Pouzoulet *et al*., 2019). If effective, this occlusion mechanism allows the plant to compartmentalize the infected zone and to generate new tissue around it (CODIT model, Pearce, 1996). Because tyloses can potentially interfere with the hydraulic functioning of the plant, they could exacerbate disease symptoms (Talboys, 1972). Tyloses are usually observed in close proximity to pathogens, as shown in artificial inoculation studies (Czemmel *et al*., 2015; Rioux *et al*., 2018, among others). However, pathogens frequently proliferate in perennial organs without physically reaching the leaves, thus leaf symptoms are often induced at a distance (Beckmann and Roberts, 1995). A recent study shows that tyloses can be present in symptomatic leaves at a distance from the pathogen niches resulting in decreased leaf hydraulic conductivity (Bortolami *et al*., 2019).

Over the last decades, grapevine (*Vitis vinifera* L.) mortality and yield loss have been reported in European, American, and South African vineyards due to esca trunk disease (Cloete *et al*., 2015; Guerin-Dubrana *et al*., 2019). Esca, a vascular disease caused by the infection of multiple fungal pathogens, affects mostly mature grapevines (more than seven-years-old), and symptoms include trunk necrosis and leaf symptoms, consisting of "tiger-stripe" necrosis and leaf wilting (Lecomte *et al*., 2012; Claverie *et al*., 2020), which are not regularly expressed season-to-season even within individual vines (Guerin-Dubrana *et al*., 2013; Li *et al*., 2017). While the pathogens responsible for esca-induced trunk necrosis have been identified (Morales-Cruz *et al*., 2018; Brown *et al*., 2020), the underlying mechanisms of leaf and fruit symptoms, and plant death are still poorly understood. Bortolami *et al*. (2019) demonstrated that the two vascular pathogens related to esca (*Phaeomoniella chlamydospora* and *Phaeoacremonium minimum*) were never detected in leaves or in stems of the current year, but always in the trunk (independently from leaf symptom presence). They further showed that esca symptomatic leaves presented significant losses in hydraulic conductivity due to the occlusion of the xylem conduits by tyloses. Together, these results reveal that esca impacts leaf hydraulic functioning, but whether or not there is a corresponding failure in perennial organs, and the exact timing of this phenomenon, are still unknown. As stems and branches are the direct connections between the pathogen niche in the trunk and the observed symptoms in the leaves, the study of stem xylem integrity is crucial in the understanding of esca impact on grapevine physiology in the current year and across seasons.

110 In this study, we investigated stem xylem integrity in grapevine during esca leaf symptom
111 formation asking the following questions: (i) Can esca lead to hydraulic failure in perennial
112 organs? (ii) Does stem hydraulic failure occur prior to or after leaf symptom expression, and
113 does it depend on xylem anatomy? (iii) Do long-term symptomatic plants present different
114 xylem anatomy and levels of hydraulic failure from long-term asymptomatic plants? To answer
115 these questions, we transplanted 28-years-old grapevines (*Vitis vinifera* L. cv Sauvignon blanc)
116 from the field into pots to transport, manipulate, and study naturally esca-infected vines. We
117 coupled *in vivo* visualizations of stem xylem functionality (using synchrotron-based X-ray
118 microcomputed tomography) with stem specific hydraulic conductivity measurements (k_s),
119 theoretical hydraulic conductivity estimates (k_{th}), optical observations of vessel occlusions, and
120 pathogen detection during symptom appearance, while comparing plants with different
121 symptom history record.

122

123 # MATERIALS AND METHODS

124 ## Plant material

125 *Vitis vinifera* cv. Sauvignon blanc grafted onto 101-14 MGt were uprooted in winter 2017,
126 2018, and 2019 from a vineyard planted in 1992 located at INRAE Bordeaux-Nouvelle
127 Aquitaine (44°47'24.8"N, 0°34'35.1"W) and transferred into pots. Following plant excavation,
128 the root system (around 0.125 m3) was immersed under water overnight, and powered with
129 indole-3-butyric acid. The plants were potted in 20l pots in fine clay medium (Klasmann
130 Deilmann substrate 4:264) and placed on heating plates at 30 °C for two months. Plants were
131 then moved to a greenhouse, under natural light conditions, and watered with nutritive solutions
132 (0.1 mM NH4H2PO4, 0.187 mM NH4NO3, 0.255 mM KNO3, 0.025 mM MgSO4, 0.002 mM
133 Fe, and oligo-elements [B, Zn, Mn, Cu, and Mo]) until the end of experiment. Since the
134 plantation these plants have been trained with a double Guyot system. This training system
135 requires a permanent main trunk and one cane on each side of the trunk which is left every year
136 to carry the buds that will produce the stems of the year. During the growing season, the stems
137 of the current year were trimmed at 1.5-2m, the secondary stems and inflorescences were
138 removed just after bud-break. Each of these plants has been surveyed each year in the field
139 since 2012 for esca leaf symptom expression following Lecomte *et al*. (2012), and has been
140 classified yearly as leaf-symptomatic or asymptomatic. Plants were then classified by their

141 long-term symptomatology record: plants asymptomatic from 2012 to 2018 (pA, previously
142 asymptomatic), and plants that have expressed symptoms at least once between 2012 and 2018
143 (pS, previously symptomatic).

144 **Esca symptom notation**

145 The evolution of esca leaf symptoms was surveyed twice a week from June to October 2019
146 on every plant (n=84, Fig. 1). As presented in Fig. 1A, esca symptoms were scored at the stem
147 and whole plant scales. The stems of the current year collected for analyses (both hydraulic
148 measurements or microCT observations) could be noted as: asymptomatic (green leaves and
149 apparently healthy), pre-symptomatic (leaves presenting yellowing or small yellow spots
150 between the veins), tiger-stripe (typical pattern of esca leaf symptoms), or apoplectic (leaves
151 passing from green to wilted in a couple of days). Along the experimentation, entire plants
152 could be noted as asymptomatic (control) or symptomatic (when at least 25% of the canopy
153 was presenting tiger-stripe leaf symptoms). At the end of the experiment (week 40, October
154 2019) each plant was classified as symptomatic or asymptomatic (control). We were then able
155 to group each stem measured into six different groups (Fig. 1A): one group of stems from
156 control plants (asymptomatic from June to October) and five groups of stems from
157 symptomatic plants: two before symptom appearance (asymptomatic and pre-symptomatic
158 stems); and three after symptom appearance (asymptomatic, tiger-stripe, and apoplectic stems).
159 To clearly differentiate asymptomatic stems collected from symptomatic plants and
160 asymptomatic stems collected from asymptomatic plants, we considered plants (and their
161 stems) that didn't show leaf symptoms during the experiment as control plants (or stems). We
162 investigated whether symptom expression (final symptom notation in October 2019, see Fig.
163 1) differed between plants with contrasted long-term symptom history (previously
164 asymptomatic vs previously symptomatic, Table 1) using a Chi-square test of independence.

165

166 **X-ray microCT observation**

167 Synchrotron-based microCT was used to visualize the content of vessels and their functionality
168 in esca tiger-stripe and control stems. Three symptomatic plants (presenting tiger-stripe
169 symptoms for 8, 7, and 3 weeks), and one asymptomatic-control plant were brought to the
170 PSICHE beamline (King *et al*., 2016) at SOLEIL synchrotron facility in September 2019.
171 Stems of the current year (ca. 2 m long) were cut under water and transferred into a solution

172 containing 75mM of contrasting agent iohexol. The iohexol solution absorbs X-rays very
173 strongly and appears bright white in X-ray scans above the iodine K-edge at 33.2 keV, and,
174 once it has been taken up by the transpiration stream, the effective functionality of each vessel
175 can be confirmed (Pratt and Jacobsen, 2018; Bortolami *et al.*, 2019). These stems were moved
176 and left outdoor to transpire the solution for at least half a day. The stems were then transferred
177 to the beamline stage and scanned twice in less than 5 minutes using two different energies of
178 a high-flux (3 x 10^{11} photons mm^{-2}) monochromatic X-ray beam: 33.1 keV and 33.3 keV. The
179 projections were recorded with a sCMOS camera equipped with a 250-mm-thick LuAG
180 scintillator (Orca Flash, Hamamatsu, Japan). The complete tomographic scan included 1500
181 projections, and each projection lasted 50 ms. Tomographic reconstructions were performed
182 using PyHST2 software (Mirone *et al.*, 2014) using the Paganin method (Paganin *et al.*, 2002),
183 resulting in 32-bit volume reconstructions of 2048 x 2048 x 1024 voxels. The final spatial
184 resolution was 2.8769 μm^3 $voxel^{-1}$.

185 **Image analysis of microCT scans**

186 The contrast agent iohexol allowed us to distinguish in intact scans the effective functionality
187 of each vessel. In the absence of iohexol, X-ray microCT scans are used to distinguish air-filled
188 vessels (appearing black, corresponding to native PLC) from sap-filled vessels (appearing
189 grey). The addition of iohexol in the xylem sap allows to distinguish the functional vessels
190 (they appear bright white when they transport the sap), from the non-functional ones (i.e.
191 occluded vessels remaining grey, corresponding to occlusion PLC). We could also observe
192 partially occluded vessels (i.e. vessels with simultaneous presence of air and occlusions, or sap
193 and occlusions). This specific case was observed by checking the presence of any occlusion in
194 at least 200 slices in each volume. Partially occluded vessels were considered as occluded,
195 some examples are presented in Fig. S1. The equivalent-circle diameter of air-filled, occluded,
196 and functional (iohexol-filled) vessels was measured on the cross sections from the central slice
197 of the microCT scanned volume using ImageJ software (Schneider *et al.*, 2012). In the high
198 energy scans recorded at 33.3 keV X-ray beam, iohexol appears bright white but its contrast
199 can sometimes impede the clear limit of the vessel lumen. Therefore, all vessel diameters were
200 recorded on the scan recorded at low energy (33.1 keV X-ray beam), then the distinction of
201 occluded from iohexol-filled vessels was done on the high energy scan (as done by Bortolami
202 et al. 2019). The theoretical hydraulic conductivity of each vessel (k_{vessel}) [kg m MPa^{-1} s^{-1}] was
203 calculated using the Hagen-Poiseuille equation:

204 $$k_{vessel} = \frac{(\pi \times Ø^4 \times \rho)}{(128 \times \eta)}$$

205 Where: $Ø$ is the equivalent circle diameter [m], ρ the density of water [998.2 kg m-3 at 20°C],
206 and η the viscosity of water [1.002 x 10-9 MPa s at 20°C]. The percentage loss of hydraulic
207 conductivity given by native air embolism (native PLC) was calculated by the ratio between
208 the hydraulic conductivity of air-filled vessels and the whole-stem hydraulic conductivity:

209 $$\text{Native PLC (\%)} = 100 \times \frac{(\sum k_{air-filled\ vessels})}{(\sum k_{\text{all vessels}})}$$

210 The percentage loss of hydraulic conductivity given by occlusions (occlusion PLC) was
211 calculated by the ratio between occluded (plus partially occluded) vessels and the whole-stem
212 hydraulic conductivity:

213 $$\text{Occlusion PLC (\%)} = 100 \times \frac{(\sum k_{\text{occluded vessels}} + \sum k_{\text{partially occluded vessels}})}{(\sum k_{\text{all vessels}})}$$

214

215 The total percentage loss of hydraulic conductivity (total PLC) was obtained by summing
216 native PLC with occlusion PLC in each sample. As the first ring of xylem vessels (i.e.
217 protoxylem) was always non-functional (>90% PLC), both in control and tiger-stripe stems, it
218 was removed from the analysis.

219 We investigated whether native PLC, and occlusion PLC differed between control and esca
220 tiger-stripe plants, using two independent generalized mixed linear models where plants were
221 treated as a random effect. Proportional data (ranging from 0 to 1, dividing all PLC values by
222 100) was analyzed to fit a logit link function and binomial distribution as appropriate.

223

224 **Monitoring stem hydraulic properties over time**

225 Xylem integrity was monitored over time by measuring hydraulic properties in stems produced
226 on the year of the experiment and collected on control and symptomatic plants along the season
227 and during esca development. Specific hydraulic conductivity (k_s) was measured on internodes
228 sampled in the center of the collected stem by the gravity method (Sperry *et al.*, 1988), and

229 compared to its theoretical analog (k_{th}) calculated from xylem anatomical observations on the
230 same internode or on the one below (see the method described below). When there are observed
231 differences in k_s among stems, comparisons with theoretical maximums (k_{th}) can show if lower
232 k_s values result from anatomical differences (i.e. different vessel size distributions) or by
233 hydraulic failure (in the case of similar vessel size and density). If k_s varies in unity with k_{th},
234 differences in k_s might result from anatomical differences (e.g. smaller k_s are related to smaller
235 vessels), otherwise k_s variations are the consequence of hydraulic failure. Each method to
236 measure k_s, k_{th}, and to observe tyloses is described below.

237 Sampling started on June 19th and finished on September 13th 2019 for a total of 10 sampling
238 dates, 39 stems of the current year from 23 control-asymptomatic plants, and 49 stems of the
239 current year from 17 symptomatic plants. We randomly sampled control plants and esca
240 symptomatic plants all along the season through the evolution of esca symptoms, obtaining
241 measurements from 14 weeks before until 10 weeks after symptom appearance. To explore the
242 contribution of the experimental design to data analysis, we tested the effect of the year of
243 uprooting (2018 and 2019), the position of the analyzed internode, and the week of the
244 measurement (i.e. evolution during the season) on k_s and k_{th} in control plants using separate
245 generalized linear mixed model with normal distributions and the plant treated as a random
246 variable (Table S1). A significant impact of the year of uproot was found for k_s and k_{th} values
247 in control plants (Table S1). This could have resulted from the more favorable conditions (i.e.
248 climatic stability and nutrient availability) for the greenhouse grown vines (note that plants
249 uprooted in 2017 were only esca symptomatic and were not included in this analysis). However,
250 once k_s and k_{th} are plotted together (Fig. S2), all the values lie on the same regression line
251 without generating outlier values (smaller k_s values correspond to smaller k_{th} values
252 independently of the uprooting year).

253 ***Stem specific hydraulic conductivity* (k_s)**

254 k_s measurements were performed on one internode per stem, located in the center of the
255 collected >1.5m long stem, following Torres-Ruiz *et al.* (2012) gravity method. In the early
256 morning, each stem was cut at the base under water to avoid air entrance in the stem, maintained
257 under water and brought to the laboratory. Hydraulic conductivity measurements were always
258 done before noon, in order to minimize the delay (never more than four hours) from the cut to
259 the measure. In the laboratory, a representative internode between the 4th to the 10th internode
260 from the base (i.e. in the center of the stem) was cut underwater with a clean razor blade, the

261 ends wrapped in tape, and the internode was connected to a pipe system. A flow of 20 mM KCl
262 solution passed through the sample from a reservoir to a precision electronic balance
263 (AS220.R2, RADWAG, Radom, PL) recording the weight every 5 seconds using the
264 WinWedge v3 5.0 software (TAL Technologies, Philadelphia, PA, USA). The solution was
265 passed through the stem at four increasing pressures (ranging from 0.001 to 0.005 MPa),
266 controlled by raising the source height. The average flow for each pressure step was determined
267 after stabilization at a steady-state as the average of 10-15 measures. Hydraulic conductance, k
268 [kg s^{-1} MPa^{-1}] was obtained by the slope generated by the flow and the corresponding pressure.
269 The linear relationship between flow and pressure obtained were always characterized by
270 R^2>0.97. Stem specific hydraulic conductivity, k_s [kg s^{-1} MPa^{-1} m^{-1}], was calculated as follows:

271 $$k_S = \frac{(k \times l)}{A}$$

272 $$A = (\left(\frac{d_1}{2}\right)^2 \times \pi) - (\left(\frac{d_2}{2}\right)^2 \times \pi)$$

273 Where: k is the hydraulic conductance, l is the length of the sample, A is the xylem area, d_1 is
274 the external diameter of the debarked stem, and d_2 is the diameter of the central pith.

275 ***Stem theoretical hydraulic conductivity (k_{th}), vessel anatomy, and tylose observation***

276 Just before hydraulic conductivity (k_s) measurements, the lower internode was stored at 4 °C
277 in 80% ethanol for analysis of xylem anatomy. When possible, the same internode of k_s
278 measurements was used for anatomical analysis and k_{th} estimations, otherwise the stored
279 internode was used for the following protocol. 50 µm thick slices were obtained using a GSL-
280 1 microtome (Gärtner *et al.*, 2014). Slices were stained using a 0.5% safranin solution during
281 5 minutes, and then washed three to four times in ethanol (100%). They were quickly soaked
282 in xylene and mounted on microscope slides with Permount Mounting Medium (Electron
283 Microscopy Science, Hatfield, PA, USA). Images were captured with a stereo microscope
284 SMZ1270 (Nikon, France) mounted with a DS-Fi3 camera (Nikon, France). The theoretical
285 conductivity of each vessel (k_{vessel}) [kg m Mpa^{-1} s^{-1}] was calculated using the Hagen-Poiseuille
286 equation as described above.

287 Where $Ø$ is the equivalent circle diameter [m] (measured with ImageJ software), ρ the density
288 of water [998.2 kg m^{-3} at 20 °C], and η the viscosity of water [1.002 x 10^{-9} MPa s at 20 °C]. k_{th}

289 of the stem [kg s^{-1} m^{-1} Mpa^{-1}] was then calculated by summing every k_{vessel} in the xylem area
290 (A) [m²]:

291 $$k_{th} = \frac{\sum k_{vessel}}{A}$$

292 In the entire cross section of each sample, the physical presence (or absence) of tyloses in vessel
293 lumina was visually assessed.

294 Regarding the statistical analysis, stems were grouped in six different categories following their
295 esca symptomatology (as presented in Fig. 1A). We investigated whether k_s, k_{th}, and total vessel
296 density differed among these different categories, and how k_s, k_{th}, and total vessel density
297 differed between stems with and without tyloses (independently from leaf symptom presence),
298 using independent mixed linear general models. The symptom / tylose category and the year
299 of uprooting (since it had a significant impact on k_s and k_{th} in control plants, Table S1) were
300 entered as fixed effects, with the plant treated as a random effect since different stems were
301 sometimes analyzed from the same plant (88 analyzed stems on 40 different plants). Total
302 density and densities for each vessel diameter class were log-transformed prior to analysis to
303 fit normality requirements. For the classes with no vessels (e.g. samples without vessel
304 diameters above 160 µm), a minimal density of 0.0001 was assigned prior to log
305 transformation. We investigated whether the frequency of symptomatic stems presenting
306 tyloses changed with the symptom age (i.e. weeks between first symptom detection and k_s
307 measurements on the same plant) with a Chi-square test. The relationships between stem k_s and
308 k_{th} were tested using linear regression models. Finally, we investigated whether k_s and k_{th} in
309 control stems differed between plants with different symptom history records using
310 independent mixed linear general models with the plant treated as a random effect.

311

312 **Fungal detection**

313 Detection and quantification of *Phaeomoniella chlamydospora* and *Phaeoacremonium*
314 *minimum* were performed using qPCR in a subsample of stems of the current year (n = 28) and
315 perennial trunks (n = 20 plants) from the same symptomatic and control plants used for
316 hydraulic and anatomical measurements. All along the season, basal internodes, from the same
317 stems sampled for k_s and k_{th} measurements, were directly placed in liquid nitrogen and stored

318 at -80 °C. At the end of the experiment, a subset of plants was cut at the base for trunk sampling.
319 A 2 cm high section was cut with a sterilized hand saw. The bark was removed and the different
320 tissues of each section (necrotic and apparently healthy wood) were separately collected using
321 ethyl alcohol-sterilized shears in a sterile environment, and immediately placed in liquid
322 nitrogen. All samples were ground in liquid nitrogen using a tissue lyser (Tissuelyser II,
323 Qiagen, Germantown, MD, USA). DNA was extracted from 60mg of ground tissue using the
324 Invisorb Spin Plant Mini Kit (Invitek GmbH, Berlin, Germany)according to the manufacturer's
325 instructions. . Detection and quantification of *P. chlamydospora* and *P. minimum* (previously
326 named *P. aleophilum*) DNA by qPCR (SYBR Green assays) was conducted using the primer
327 sets PchQF (5'-CTCTGGTGTGTAAGTTCAATCGACTC-3')/PchQR (5'-
328 CCATTGTAGCTGTTCCAGATCAG-3') and PalQF(5'-
329 CCGGTGGGGTTTTTACGTCTACAG-3')/ PalQR(5'-
330 CGTCATCCAAGATGCCGAATAAAG-3') (Pouzoulet *et al*. 2013). The qPCR reactions
331 proceeded in a final volume of 25 µl, and the reaction mixtures containing 2 µL of DNA
332 template, 12.5 µl of 2X SYBRGreen Quantitect Master Mix (Qiagen, Venlo, Netherlands), and
333 each primer at a final concentration of 0.4 µM. Experiments were conducted with a Mx3005P
334 Real-Time PCR cycler using MxPro qPCR software (Agilent Technologies). The cycling
335 program, as described in Pouzoulet *et al*. (2017), consisted of an initial denaturation step at
336 95°C for 15 min, and 40 cycles of 15 s at 95°C (for denaturation) followed by 45 s at 62°C (for
337 both annealing and extension). A melting analysis of 40 min from 60 to 95° was performed to
338 verify reaction's specificity and the absence of byproducts. Preparation and use of standard
339 solutions for the absolute quantification of fungal DNA was realized following Pouzoulet *et al*.
340 (2013) using ten-fold dilutions of fungal DNA extracts obtained from axenic cultures. Reaction
341 efficiencies ranging from 90% and 95% with an $R^2 > 0.99$ (n=15) were obtained for both
342 PchQF/R and PalQF/R primer sets. The average amount of DNA was determined based on
343 three technical replicates (standards and plates) with a detection threshold superior to 95% (i.e.
344 at least three positive amplification out of three replicates) or otherwise discarded (i.e. pathogen
345 DNA was considered absent). Pathogen DNA quantity (average value of three technical
346 replicates, fg/µl) was normalized by the amount of total DNA (ng/µl), measured using a Qubit
347 fluorometer. The results from each trunk sample (i.e. necrotic or apparently healthy wood) were
348 averaged together in order to obtain one quantification per plant. We investigated whether the
349 amount of fungal DNA (both for *P. chlamydospora* and for *P. minimum*) in trunks differed
350 between symptomatic and control plants, and between control plants with different symptom

351 history records, using generalized linear mixed model with a poisson distribution and a log
352 likelihood function.

353

354 **Statistical analysis**

355 All data management and statistical tests were done in SAS software (SAS 9.4; SAS Institute).
356 We used PROC GLIMMIX for generalized linear mixed models, PROC GLM for generalized
357 linear models, PROC REG for regression analyses and PROC FREQ for frequency analyses
358 (Chi-square test of independence). The normality of the response variables was tested using a
359 Kolmogorov-Smirnov test (PROC UNIVARIATE) prior to analyses. Data were log-
360 transformed (total density) or appropriate distributions (binomial, poisson) were fitted when
361 appropriate.

362

363 # RESULTS

364 **Esca leaf symptom expression within and across seasons**

365 Esca leaf symptoms were recorded in 20 out of the 58 plants followed in this study (35%, Fig.
366 1, Table 1). The number of symptomatic plants increased gradually with time, from the first
367 symptom appearance in early June to the last in late September (Fig. 1). There was no effect of
368 the plant history (previously asymptomatic pA, or previously symptomatic pS) on 2019
369 symptom expression (n=58, X^2=0.27, P=0.60). On 20 pA plants, six (30%) expressed leaf
370 symptoms in 2019 (Table 1). On 38 pS plants, fourteen (37%) showed symptoms in 2019
371 (Table 1). However, pS plants expressed symptoms from June to the end of September, while
372 pA plants showed leaf symptoms only in September.

373

374 ***In vivo* observations of esca symptomatic stems**

375 Xylem vessels of control and tiger-stripe stems were observed using three dimensional X-ray
376 microCT scans in iohexol-fed samples (Fig. 2, 3, Table S2). As shown in Fig. 2, functional and
377 non-functional vessels can be discriminated through the use of iohexol (functional vessels
378 appear bright white, non functional vessels appear either black if air-filled or grey if occluded).

379 We observed almost totally functional stems in all asymptomatic stems (<20% total PLC, Fig.
380 2A-C), and 40% of tiger-stripe stems (e.g. Fig. 2D-G). Higher levels of PLC (>20% total PLC,
381 Fig H-M) were observed in the remaining tiger-stripe stems, with 40% of tiger-stripe stems
382 exhibiting over 50% total PLC (Fig. 2J-M). When the two components of PLC were
383 disentangled, we observed that the level of native PLC remained low both in control (6.5 ±
384 2.6%) and in tiger-stripe (12.2 ± 2.9%) stems (Fig. 3A). Occlusion PLC values were virtually
385 zero in control stems (0.7 ± 0.02%) while in tiger-stripe stems the mean occlusion PLC values
386 was 27.5 ± 8.2% (Fig. 3B). Nevertheless, the variability of occlusion PLC across tiger-stripe
387 stems was very high, the values ranging from 0.3% to 72.9% (Fig. 2D-M, and 3B), and
388 occlusion PLC was not correlated to symptom age (n=10, $F_{2,7}$=0.19, P=0.83). Consequently,
389 no statistical differences in native or occlusion PLC were found between control and tiger-
390 stripe stems (Fig. 3). When higher occlusion PLC was measured (Fig. 2H-M), occluded vessels
391 could be organized either on one side of the stem (Fig 2J-L) or randomly distributed across the
392 section (Fig 2H, 2I, 2M). In 90% of symptomatic stems, we observed that the most external
393 vessels were functional. Occlusions were present equally in all vessel diameter classes (Fig.
394 S3).

395

396 **Tylose development, stem specific (k_s) and theoretical (k_{th}) hydraulic conductivity during**
397 **esca leaf symptom formation**

398 Tyloses were identified in the xylem vessels of certain tiger-stripe stems and throughout the
399 temporal development of esca leaf symptoms, from the appearance of symptoms to 11 weeks
400 after. All apoplectic stems and 62.5% (15 of 24 analyzed stems) of esca tiger-stripe stems
401 presented tyloses, while all other stems (control, asymptomatic or pre-symptomatic) did not
402 contain these occlusions, even until one week before symptom development. In esca tiger-
403 stripe stems, tyloses were not related to specific plants, or to symptom age (i.e. on the same
404 plant at the same moment, different symptomatic stems could present tyloses, or not, n=24,
405 X^2=7.47, P=0.38).

406 Overall, no significant impact of esca symptoms was observed on k_s (Fig. 4A), even if tiger-
407 stripe stems were divided between those with and without tyloses. Control stems presented a
408 mean (± SE) k_s of 24.97 ± 1.72 kg s^{-1} MPa^{-1} m^{-1}; all the stems without tyloses measured on
409 symptomatic plants showed the same range of values as control stems (Fig 4A, Table 2): 26.04

410 ± 4.71 for asymptomatic before symptoms appearance, 30.32 ± 4.26 for pre-symptomatic
411 stems, 19.80 ± 5.18 for asymptomatic stems after symptom appearance on the plant, and 21.29
412 ± 5.40 for tiger-stripe stems without tyloses. Stems with tyloses (tiger-stripe and apoplectic
413 stems) presented the lowest average k_s values (11.27 ± 2.86 and 2.47 ± 1.45 kg s^{-1} MPa^{-1} m^{-1}
414 for tiger-stripe and apoplectic, respectively). Regarding k_{th}, no significant impact of esca
415 symptoms was found (Fig. 4C, Table 2), all the values were in the same range, with average
416 values ranging from 70.44 (for tiger-stripe stems with tyloses) to 87.88 (for pre-symptomatic
417 stems) kg s^{-1} MPa^{-1} m^{-1}.

418 In order to further investigate the impact of esca on stem hydraulics, we explored the
419 relationship between individual stem k_s and k_{th} in each symptom category (Fig. 4B, S4, Table
420 2). Significant relationships were found between k_s and k_{th} in all groups except in asymptomatic
421 stems after symptom appearance and symptomatic stems with the physical presence of tyloses
422 (Fig. S4, Table 2). The slopes of regression curves between k_s and k_{th} did not vary among
423 groups in the absence of tyloses (slope values ranged between 0.3 and 0.4, Table 2) while it
424 was close to 0 in the presence of tyloses (0.17 for tiger-stripe and 0.04 for apoplectic stems).
425 When k_s and k_{th} are compared in the presence or absence of tyloses, we observed that k_s was
426 significantly lower when tyloses were present (9.81 ± 2.51 kg s^{-1} MPa^{-1} m^{-1} in the presence of
427 tyloses vs 25.06 ± 1.46 kg s^{-1} MPa^{-1} m^{-1} in the absence of tyloses, Table 2, n=88, $F_{1,49}$=7.11,
428 P=0.01) while k_{th} did not significantly differ. Stems without tyloses presented a strong
429 correlation between k_s and k_{th}, while in the presence of tyloses this relationship was not
430 significant (Table 2, Fig. 4B).

431 Total vessel density did not significantly differ between stem symptomatology (comparing all
432 the seven categories presented in Table 2), even when vessel density was partitioned by vessel
433 diameter classes (Fig. 4D).

434 Finally, we tested the impact of disease history (comparing pA and pS plants) on the hydraulic
435 conductivity and xylem anatomy in control plants. There were no differences between long-
436 term symptomatic (pS) and long-term asymptomatic (pA) plants in stem k_s, stem k_{th}, or total
437 vessel density (Table 3).

438

439 **Fungal detection**

440 The two vascular pathogens associated with esca (*Phaeomoniella chlamydospora* and
441 *Phaeoacremonium minimum*) were never detected in stems of the current year while they were
442 systematically detected in the perennial trunk of both control and symptomatic plants (Table
443 4). In trunks, a significantly higher quantity of fungal DNA was detected in tiger-stripe
444 symptomatic plants than in controls (Table 4). We found 2.14- and 1.64-fold more of *P.*
445 *chlamydospora* and *P. minimum* DNA in symptomatic trunks relative to controls. In control
446 plants, different symptom history records impacted the quantity of fungal DNA detected by
447 qPCR, for *Phaeomoniella chlamydospora*, and for *Phaeoacremonium minimum*. We found
448 1.65- and 2.84-fold more *P. chlamydospora* and *P. minimum* DNA in previously symptomatic
449 trunks relative to previously asymptomatic trunks (Table 3).

450

451 # DISCUSSION

452 Our results regarding the impact of esca on stem xylem integrity show that the presence of
453 plant-derived tyloses induced hydraulic failure in 60% of symptomatic stems of the current
454 year. Tyloses were only observed in symptomatic stems, and resulted in more than 50% PLC
455 in 40% of the stems, unrelated to symptom age. We demonstrated that the presence of leaf
456 symptoms during previous seasons had no impact on the likelihood of symptom appearance in
457 the current year, or on stem hydraulic conductivity and xylem anatomy. Vascular fungi were
458 never detected in the same organs as the tyloses (stems of the current year), and although they
459 were present in trunks of both tiger-stripe and control plants, tiger-stripe plants showed higher
460 quantities of fungal DNA. Among control plants that did not express symptoms in the year of
461 the study, we found higher quantities of fungal DNA in trunks of those plants with a long-term
462 history of symptom formation. Albeit xylem occlusions were not observed in the totality of
463 tiger-stripe stems, they could amplify yield loss plant mortality, especially in the context of
464 climate change as they impair water transport in a majority of symptomatic stems.

465

466 ## *In vivo* xylem integrity observations and hydraulic vulnerability segmentation

467 Using direct X-ray microCT imaging in esca symptomatic stems, we found that hydraulic
468 conductivity loss was almost entirely associated with the presence of tyloses. Different studies
469 have investigated the link between vascular pathogen development and hydraulic conductivity

470 in stems (Collins *et al*., 2009; Lachenbruch and Zhao, 2019; Mensah *et al*., 2020). During biotic
471 stresses, air embolisms have been shown to decrease hydraulic conductivity during bacterial
472 leaf scorch disease (McElrone *et al*., 2003; 2008), Pierce's disease (Pérez-Donoso *et al*., 2016),
473 and Pine wilt disease (Yazaki *et al*., 2018). In the case of fungal wilt diseases, the hydraulic
474 conductivity loss was associated with nongaseous embolism (i.e. tyloses) at the point of
475 pathogen inoculation (Guerard *et al*., 2000; Sallé *et al*., 2008; Beier *et al*., 2017; Mensah *et al*.,
476 2020), or with canker presence in naturally infected stems (Lachenbruch and Zhao, 2019).

477 Using iohexol we were able to visually observe the exact spatial organization of functional
478 vessels. Interestingly, in some symptomatic samples we found functional vessels surrounding
479 the non-functional xylem (Fig. 2J-L), suggesting that the plant was able to preserve the more
480 external vessels from occlusions or to form new functional vessels after the loss of
481 conductivity. Moreover, the sectoriality of the occlusions observed in Fig. 2J-L was
482 reminiscent of the sectoriality observed in the distributions of trunk necrosis, especially on the
483 brown stripe necrosis appearing along the vasculature (Lecomte *et al*., 2012).

484 Comparing these results with our precedent study using the same technique in leaves, we
485 showed that esca symptomatic leaves presented higher levels of occlusion PLC (61 ± 7% in
486 midribs, and 54 ± 9% in petioles, data from Bortolami *et al*., 2019) compared to stems (27 ± 8
487 %, occlusion PLC), suggesting hydraulic vulnerability segmentation (although PLC in leaves
488 and stems were measured in different plants and years). The hydraulic segmentation theory
489 relies on the fact that annual organs (i.e. leaves) are more vulnerable than perennial organs (i.e.
490 stems) to drought induced air embolism (Tyree and Ewers, 1991). Grapevine is well known for
491 exhibiting strong hydraulic vulnerability segmentation (Charrier *et al*., 2016; Hochberg *et al*.,
492 2016; 2017). This is thought to be adaptive, where the higher vulnerability in leaves and
493 petioles favors embolism formation and leaf shedding prior to embolism formation in stems,
494 thus protecting the perennial organs. Our observations during esca pathogenesis demonstrate
495 that, analogous to the hydraulic vulnerability segmentation theory, leaves appear more
496 vulnerable to the formation of nongaseous embolism as well, which could mitigate the risk of
497 hydraulic failure in perennial organs. From another perspective, the difference may not be a
498 direct effect of the specific organ's vulnerability to nongaseous embolism, but a consequence
499 of a difference in the accumulation of putative toxins and/or elicitors. Indeed, we confirmed
500 here that esca leaf symptoms occur at a distance from the pathogen niche because vascular
501 pathogens were never detected in stems of the current year, suggesting that the plant may

502 transport a signal (i.e. toxins or elicitors) from the infected trunk up to the leaves. If the signal
503 accumulates in leaves in a higher amount than it does in the stems (water potentials are more
504 negative in leaves compared to stems), and stimulates occlusion formation, stems would then
505 be secondarily affected.

506

507 **Hydraulic conductivity, tyloses, and vessel anatomy**

508 Tyloses could have different impacts, both positive and negative, during wilt disease
509 pathogenesis: (i) tyloses contribute to pathogen resistance as they aim to seal off vessel lumens
510 and impede pathogens spread throughout the host (CODIT model, Shigo, 1984). This is the
511 case regarding the susceptibility of different species or varieties to specific pathogens (Jacobi
512 and MacDonald, 1980; Ouellette *et al*., 1999; Clérivet *et al.,* 2000; Et-Touil *et al*., 2005;
513 Venturas *et al*., 2014; Park and Juzwik 2014; Rioux *et al*., 2018), in particular to *Phaeomoniella*
514 *chlamydospora*, one of the pathogen associated with esca (Pouzoulet *et al*., 2017; 2020). (ii) In
515 other studies, it has been shown that tyloses can exacerbate symptoms (Talboys, 1972): they
516 cause a reduction in stem hydraulic conductivity, sometimes associated with a reduction in
517 stomatal conductance in leaves and, in the most severe cases, wilting (Parke *et al*., 2007; Beier
518 *et al*., 2017; Lachenbruch and Zhao, 2019, Mensah *et al*., 2020 during fungi development; Sun
519 *et al*., 2013; Deyett *et al*., 2019 during Pierce's disease). Our results suggest that during esca
520 tyloses might lead to symptom exacerbation. Esca has also been suggested to lead to a general
521 reduction in xylem water transport and stomatal conductance (Ouadi *et al*., 2019), and tyloses
522 could be a major contributor to these phenomena as during winter senescence (Salleo *et al*.,
523 2002; Sun *et al*., 2008). However, when symptomatic stems have no tyloses (~37% of the stems
524 with tiger-stripe symptoms), esca leaf symptom formation seems to arise from within the leaf
525 itself, and may not result from upstream hydraulic failure. Although tyloses were never
526 detected in asymptomatic stems prior to the onset of leaf symptoms, the time sequence of tylose
527 and leaf symptom development has still to be determined. Since both the microCT and
528 anatomical observations visualize relatively narrow regions of the stems, tylose presence could
529 have been underestimated (i.e. if there was additional tylose development up or downstream of
530 the stem sections visualized). However, it should be pointed out that if significant
531 underestimation were present we would expect some loss of conductivity even in internode
532 sections from which we observed no tyloses in the sampled cross sections. At least when

533 considering a single internode our direct hydraulic conductivity measurements do not support
534 the hypothesis that tyloses were underestimated (Fig. 4B).

535 Xylem is the battleground between vascular pathogens and the plant's defense response
536 (Yadeta and Thomma, 2013). Even if xylem vessel anatomy is less investigated, it could have
537 a crucial role in plant resistance and response to vascular pathogens. For example, during Dutch
538 elm wilt disease (due to *Ophiostoma spp.*) the most sensitive species and varieties present wider
539 xylem vessels (Elgersma, 1970; Mcnabb *et al*., 1970; Solla and Gil 2002; Pita *et al*., 2018).
540 Smaller vessels could occlude faster, sustaining a more efficient pathogen restriction (Venturas
541 *et al*., 2014). Our results on xylem vessel anatomy suggest that stems with tyloses tend to
542 present higher densities of small vessels, even if we did not observe any differences in total k_{th}
543 values and microCT scans showed that occlusions appear randomly in every vessel size class
544 (Fig. S3). It could be possible that tylose formation might be interfering with stem water
545 relations reducing the carbohydrates available for plant growth, producing smaller vessels in
546 stems of symptomatic plants. In contrast, artificial inoculations showed that xylem vessel
547 diameter had a strong impact on esca-related vascular pathogen development (Pouzoulet *et al*.,
548 2017; 2020), and in the kinetic of vessel occlusion in grapevine stems (Pouzoulet *et al*., 2019).
549 The relationships between esca leaf symptoms, xylem anatomy, and tylose presence should be
550 studied in detail in trunks, where vascular pathogens are present, and among different grapevine
551 varieties and rootstocks as they are known to show different susceptibility to symptom
552 expression.

553

554 **Long-term consequences of esca on leaf symptom expression and stem hydraulic integrity**

555 In field surveys, esca leaf symptoms are often randomly distributed spatially throughout
556 vineyards and are not consistent from season to season in individual vines (Mugnai *et al*., 1999;
557 Surico *et al*., 2000; Marchi *et al*., 2006; Guerin-Dubrana *et al*., 2013; Li *et al*., 2017). However,
558 esca-related vine death is strongly related to leaf symptoms as death is usually observed
559 following a year with symptom expression (Guerin-Dubrana *et al*., 2013). In agreement with
560 these field studies, we observed similar percentages of symptomatic plants between those that
561 had already expressed esca symptoms in the past (from one to seven consecutive years, pS
562 plants), and those that had never expressed symptoms over the past seven years (pA plants).
563 However, we also found that pS plants expressed symptoms earlier in the season than pA

564 plants, suggesting that symptoms might require more time to develop in pA plants. We did not
565 find any significant differences in k_s and k_{th} values between plants with contrasted long-term
566 symptom history. This result suggests that esca leaf symptoms may have xylem anatomical
567 consequences within the year of expression by the production of tyloses, but not across seasons.
568 Moreover, we showed that DNA pathogen amount (*Phaeoacremonium minimum* and
569 *Phaeomoniella chlamydospora*) depends on the symptom expression in the season of sampling,
570 and on the long-term symptom history. Altogether, these results suggest that a higher amount
571 of vascular fungi in the trunk represents a higher risk in reproducing leaf symptoms, and
572 consequently, a higher risk of plant death.

573

574 **Hydraulic failure and esca leaf symptom pathogenesis**

575 Our results showed that, even if esca-related stem occlusion was extremely variable, 40% of
576 the microCT analyzed stems presented a total PLC greater than 50%. Under drought conditions
577 alone, studies suggest that grapevines are not able to recover in the current season from PLC
578 greater than 50% in stems (Charrier *et al*., 2018). Thus, to what extent these levels of esca-
579 induced hydraulic failure compromise future vine performance, and/or increase the likelihood
580 of developing esca leaf symptoms in the future remains an open question.

581 We showed that, similarly to visual leaf symptoms, tyloses in stems were generated at a
582 distance from the pathogen niche in the trunk. Comparing our results with Bortolami *et al*.
583 (2019), we show that the PLC due to the occlusions (hydraulic failure) observed using microCT
584 in leaves was on average twice higher than the PLC observed in stems in the present work. We
585 could hypothesize that, following pathogen activities in the trunk, a signal passing through the
586 xylem network and stimulating tyloses, first accumulates in leaves and then affects the stems.
587 However, the exact signal and action remain unknown, as we showed that the presence of
588 tyloses depended upon given symptomatic stems rather than symptomatic plants (i.e. two stems
589 in the same plant, with same tiger-stripe symptoms, sampled at the same moment, could or
590 could not present tyloses).

591 We showed that there were no differences in symptom expression, nor in the stem hydraulic
592 properties, regarding the long-term symptom history. We can conclude that the processes that
593 generate tiger-stripe symptoms are largely restricted to the current year of the symptom
594 expression. However, in plants expressing symptoms for the first time according to our disease

595 record, these processes could require more time, as they showed symptoms only late in the
596 season. The presence of occlusion, leading to hydraulic failure in stems, could exacerbate leaf
597 symptom expression in the following seasons, possibly contributing to death. We could
598 speculate that a stem expressing extensive hydraulic failure could be more prone to express
599 symptoms in the following year or, in the worst cases, to die. If the level of hydraulic failure
600 could affect the stem mortality in the following year, the choice of stems with a complete
601 absence of failure during the winter pruning could reduce the impact of esca in vineyards. The
602 pruning practices are known to impact the course of infection and leaf symptom development
603 and it has been shown that trunk renewal could be an effective management practice to prevent
604 grapevine trunk diseases in the vineyard (Travadon *et al*. 2016, Kaplan *et al*. 2016, Gramaje *et*
605 *al*. 2018). In addition, the presence of occlusions could also amplify plant susceptibility to
606 drought-induced hydraulic failure, enhancing the risk of plant mortality in the field as
607 suggested by McDowell *et al*. (2008). It could be speculated that a decrease in soil water
608 potential or a high evaporative demand, concomitant to esca-induced hydraulic failure, could
609 embolize the remaining functional xylem vessels stopping the water flow and desiccating plant
610 tissues (this could be the case in apoplectic plants for example). In perspective, future studies
611 should investigate the link between pathogen activities and occlusion development, especially
612 in trunks, and the subsequent hydraulic failure consequences on whole plant physiology.

613 **SUPPORTING INFORMATION**

614 The following Supporting Information is available for this article:

615 **Fig. S1**. Two-dimensional reconstruction of longitudinal cross sections from X-ray microCT
616 volumes of grapevine stems.

617 **Fig. S2**. Relationship between k_s and k_{th} in control plants.

618 **Fig. S3**. Vessel density and percentage of occluded vessels in tiger-stripe stems for different
619 vessel diameter classes.

620 **Fig. S4**. Relationships between k_s and k_{th} in each stem symptom category.

621 **Table S1**. Effect of year of uprooting, internode analyzed, and sampling date on k_s and k_{th} in
622 control stems.

623 **Table S2.** Calculated theoretical hydraulic conductivity (k_{th} %), and hydraulic conductivity loss
624 (PLC %) from X-ray microCT volumes of intact grapevine stems.

625

626

DATA AVAILABILITY STATEMENT

Raw datasets are available in the INRAE dataverse: Bortolami, Giovanni; Farolfi, Elena; Badel, Eric; Burlett, Regis; Cochard, Herve; Ferrer, Nathalie; King, Andrew; Lamarque, Laurent J.; Lecomte, pascal; Marchesseau-Marchal, Marie; Pouzoulet, Jerome; Torres-Ruiz, Jose M.; Trueba, Santiago; Delzon, Sylvain; Gambetta, Gregory A.; Delmas, Chloe E.L., 2021, "Raw data for the paper "Seasonal and long-term consequences of esca on grapevine stem xylem integrity"", https://doi.org/10.15454/U9KJEW, Portail Data INRAE, V1.

ACKNOWLEDGMENTS

We thank the experimental teams of UMR SAVE and UMR EGFV (Bord'O platform, INRAE, Bordeaux, France) and the SOLEIL synchrotron facility (beamline PSICHE) for providing the materials and logistics. Specifically, we thank Jérôme Jolivet and Sebastien Gambier (UMR SAVE) for providing technical knowledge and support for plant transplantation and maintenance. This work was supported by the French Ministry of Agriculture, Agrifood, and Forestry (FranceAgriMer and CNIV) within the PHYSIOPATH project (program Plan National Dépérissement du Vignoble, 22001150-1506) awarded to C.E.L.D., and program Investments for the Future (ANR-10-EQPX-16, XYLOFOREST).

AUTHOR CONTRIBUTIONS

C.E.L.D., G.A.G., G.B., and S.D. designed the experiments;

E.F., G.A.G., S.D., E.B., R.B., H.C., A.K., L.J.L., J.M.T.-R., S.T. participated in synchrotron campaigns;

G.B., C.E.L.D., E.F., and N.F. conducted the esca symptom notations;

G.B., M.M.-M.,and N.F. conducted the histological observations;

E.F. conducted the hydraulic conductivity measurements and participated to data analyses;

N.F., and J.P., conducted the pathogen detection;

G.B. analyzed the microCT, optical images, and analyzed the data;

P.L. provided data on disease history of the plants;

G.B., C.E.L.D., and G.A.G. wrote the article;

all authors edited and agreed on the last version of the article

REFERENCES

Akpaninyang FE, Opara EU. 2017. The Influence of Toxins in Disease Symptom Initiation in Plants: A Review. Journal of Agriculture and Sustainability 10, 29-52.

Aleemullah M., Walsh K. 1996. Australian papaya dieback: Evidence against the calcium deficiency hypothesis and observations on the significance of laticifer autofluorescence. Australian Journal of Agricultural Research 47, 371-385.

Alvindia DG, Gallema FLM. 2017. *Lasiodiplodia theobromae* causes vascular streak dieback (VSD)–like symptoms of cacao in Davao Region, Philippines. Australasian Plant Disease Notes 12, 54.

Anderegg WRL, Kane JM, Anderegg LDL. 2013. Consequences of widespread tree mortality triggered by drought and temperature stress. Nature Climate Change 3, 30-36.

Anderegg WRL, Klein T, Bartlett M, Sack L, Pellegrini AFA, Choat B, Jansen S. 2016. Meta-analysis reveals that hydraulic traits explain cross-species patterns of drought-induced tree mortality across the globe. Proceedings of the National Academy of Sciences 113, 5024-5029.

Andolfi A, Mugnai L, Luque J, Surico G, Cimmino A, Evidente A. 2011. Phytotoxins Produced by Fungi Associated with Grapevine Trunk Diseases. Toxins 3, 1569-1605.

Beckman CH, Roberts EM. 1995. On the Nature and Genetic Basis for Resistance and Tolerance to Fungal Wilt Diseases of Plants. Advances in Botanical Research 21, 35-77.

Beier GL, Held BW, Giblin CP, Cavender-Bares J, Blanchette RA. 2017. American elm cultivars: Variation in compartmentalization of infection by *Ophiostoma novo-ulmi* and its effects on hydraulic conductivity. Forest Pathology 47, 1-11.

Bettenfeld P, Fontaine F, Trouvelot S, Fernandez O, Courty P-E. 2020. Woody Plant Declines. What's Wrong with the Microbiome? Trends in Plant Science 25, 381-394.

Bonsen KJM, Kučera LJ. (1990). Vessel Occlusions in Plants: Morphological, Functional and Evolutionary Aspects. IAWA Journal 11, 393-399.

Bortolami G, Gambetta GA, Delzon S, *et al.* (2019). Exploring the Hydraulic Failure Hypothesis of Esca Leaf Symptom Formation. Plant Physiology 181, 1163-1174.

Brown AA, Lawrence DP, Baumgartner K. 2020. Role of basidiomycete fungi in the grapevine trunk disease esca. Plant Pathology 69, 205-220.

Cailleret M, Jansen S, Robert EMR, *et al*. 2017. A synthesis of radial growth patterns preceding tree mortality. Global Change Biology 23, 1675-1690.

Charrier G, Delzon S, Domec J-C, *et al*. 2018. Drought will not leave your glass empty: Low risk of hydraulic failure revealed by long-term drought observations in world's top wine regions. Science Advances 4, 1-9.

Charrier G, Torres-Ruiz JM, Badel E, *et al*. 2016. Evidence for Hydraulic Vulnerability Segmentation and Lack of Xylem Refilling under Tension. Plant Physiology 172, 1657-1668.

Claverie M, Notaro M, Fontaine F, Wery J. 2020. Current knowledge on Grapevine Trunk Diseases with complex etiology : A systemic approach. Phytopathologia Mediterranea 59, 29-53.

Clérivet A, Déon V, Alami I, Lopez F, Geiger J-P, Nicole M. 2000. Tyloses and gels associated with cellulose accumulation in vessels are responses of plane tree seedlings (*Platanus* × *acerifolia*) to the vascular fungus *Ceratocystis fimbriata* f. Sp *platani*. Trees 15, 25-31.

Cloete M, Mostert L, Fischer M, Halleen F. 2015. Pathogenicity of South African Hymenochaetales taxa isolated from esca-infected grapevines. Phytopathologia Mediterranea 54, 368-379.

Collins BR, Parke JL, Lachenbruch B, Hansen EM. 2009. The effects of *Phytophthora ramorum* infection on hydraulic conductivity and tylosis formation in tanoak sapwood. Canadian Journal of Forest Research 39, 1766-1776.

Czemmel S, Galarneau ER, Travadon R, McElrone AJ, Cramer GR, Baumgartner K. 2015. Genes expressed in grapevine leaves reveal latent wood infection by the fungal pathogen *Neofusicoccum parvum*. PloS one 10*,* e0121828.

Desprez-Loustau M-L, Marçais B, Nageleisen L-M, Piou D, Vannini A. 2006. Interactive effects of drought and pathogens in forest trees. Annals of Forest Science 63, 597-612.

Deyett E, Pouzoulet J, Yang J-I, Ashworth VE, Castro C, Roper MC, Rolshausen PE. 2019. Assessment of Pierce's disease susceptibility in *Vitis vinifera* cultivars with different pedigrees. Plant Pathology 68, 1079-1087.

De Micco V, Balzano A, Wheeler EA, Baas P. 2016. Tyloses and gums : A review of structure, function and occurrence of vessel occlusions. IAWA Journal 37, 186-205.

Elgersma DM. 1970. Length and diameter of xylem vessels as factors in resistance of elms to Ceratocystis ulmi. Netherlands Journal of Plant Pathology 76, 179-182.

Eskalen A, Stouthamer R, Lynch SC, Rugman-Jones PF, Twizeyimana M, Gonzalez A, Thibault T. 2013. Host Range of Fusarium Dieback and Its Ambrosia Beetle (Coleoptera : Scolytinae) Vector in Southern California. Plant Disease 97, 938-951.

Et-Touil A, Rioux D, Mathieu FM, Bernier L. 2005. External symptoms and histopathological changes following inoculation of elms putatively resistant to Dutch elm disease with genetically close strains of *Ophiostoma*. Canadian Journal of Botany 83, 656–667.

Fallon B, Yang A, Lapadat C, Armour I, Juzwik J, Montgomery RA, Cavender-Bares J. 2020. Spectral differentiation of oak wilt from foliar fungal disease and drought is correlated with physiological changes. Tree Physiology 40, 377-390.

Fradin EF, Thomma BPHJ. 2006. Physiology and molecular aspects of *Verticillium* wilt diseases caused by *V. dahliae* and *V. albo-atrum*. Molecular Plant Pathology 7, 71-86.

Gärtner H, Lucchinetti S, Schweingruber FH. 2014. New perspectives for wood anatomical analysis in dendrosciences: the GSL1-microtome. Dendrochronologia 32, 47-51.

Goberville E, Hautekèete N-C, Kirby RR, Piquot Y, Luczak C, Beaugrand G. 2016. Climate change and the ash dieback crisis. Scientific Reports 6 doi:10.1038/srep35303.

Gramaje D, Úrbez-Torres JR, Sosnowski MR. 2018. Managing Grapevine Trunk Diseases With Respect to Etiology and Epidemiology : Current Strategies and Future Prospects. Plant Disease 102, 12-39.

Guérard N, Maillard P, Bréchet C, Lieutier F, Dreyer E. 2007. Do trees use reserve or newly assimilated carbon for their defense reactions? A 13C labeling approach with young Scots pines inoculated with a bark-beetle-associated fungus (*Ophiostoma brunneo ciliatum*). Annals of Forest Science 64, 601-608.

Guerin-Dubrana L, Labenne A, Labrousse JC, Bastien S, Rey P, Gegout-Petit A. 2013. Statistical analysis of grapevine mortality associated with esca or Eutypa dieback foliar expression. Phytopathologia Mediterranea 52, 276-288.

Guerin-Dubrana L, Fontaine F, Mugnai L. 2019. Grapevine trunk disease in European and Mediterranean vineyards : Occurrence, distribution and associated disease-affecting cultural factors. Phytopathologia Mediterranea 58, 49-71.

Hochberg U, Albuquerque C, Rachmilevitch S, Cochard H, David-Schwartz R, Brodersen CR, McElrone A, Windt CW. 2016. Grapevine petioles are more sensitive to drought induced embolism than stems : Evidence from *in vivo* MRI and microcomputed tomography observations of hydraulic vulnerability segmentation: Hydraulic vulnerability segmentation in grapevine. Plant, Cell & Environment 39, 1886-1894.

Hochberg U, Windt CW, Ponomarenko A, Zhang Y-J, Gersony J, Rockwell FE, Holbrook NM. 2017. Stomatal Closure, Basal Leaf Embolism, and Shedding Protect the Hydraulic Integrity of Grape Stems. Plant Physiology 174, 764-775.

Jacobi WR, MacDonald WL. 1980. Colonization of resistant and susceptible oaks by *Ceratocystis fagacearum*. Phytopathology 70, 618-623.

Kaplan J, Travadon R, Cooper M, Hillis V, Lubell, Baumgartner K. 2016. Identifying economic hurdles to early adoption of preventative practices_ The case of trunk diseases in California winegrape vineyards. Wine Economics and Policy 15, 127-141.

King A, Guignot N, Zerbino P, *et al.* 2016. Tomography and imaging at the PSICHE beam line of the SOLEIL synchrotron. Review of Scientific Instruments 87, 093704.

Lachenbruch B, Zhao J-P. 2019. Effects of phloem on canopy dieback, tested with manipulations and a canker pathogen in the *Corylus avellana/Anisogramma anomala* host/pathogen system. Tree Physiology 39, 1086-1098.

Lecomte P, Darrieutort G, Liminana J-M, Comont G, Muruamendiaraz A, Legorburu F-J, Choueiri E, Jreijiri F, El Amil R, Fermaud M. 2012. New Insights into Esca of Grapevine: The Development of Foliar Symptoms and Their Association with Xylem Discoloration. Plant Disease 96, 924-934.

Li S, Bonneu F, Chadoeuf J, Picart D, Gégout-Petit A, Guérin-Dubrana L. 2017. Spatial and Temporal Pattern Analyses of Esca Grapevine Disease in Vineyards in France. Phytopathology 107, 59-69.

Martin N, Vesentini D, Rego C, Monteiro S, Oliveira H, Ferreira RB. 2009. *Phaeomoniella chlamydospora* infection induces changes in phenolic compounds content in *Vitis vinifera*. Phytopathologia Mediterranea 48, 101-116.

Martín JA, Solla A, Ruiz-Villar M, Gil L. 2013. Vessel length and conductivity of *Ulmus* branches : Ontogenetic changes and relation to resistance to Dutch elm disease. Trees 27, 1239-1248.

McDowell N, Pockman WT, Allen CD, *et al*. 2008. Mechanisms of plant survival and mortality during drought : Why do some plants survive while others succumb to drought? New Phytologist 178, 719-739.

McElrone AJ, Sherald JL, Forseth IN. 2003. Interactive effects of water stress and xylem-limited bacterial infection on the water relations of a host vine. Journal of Experimental Botany 54, 419-430.

McElrone AJ, Jackson S, Habdas P. 2008. Hydraulic disruption and passive migration by a bacterial pathogen in oak tree xylem. Journal of Experimental Botany 59, 2649-2657.

McNabb HS, Heybroek HM, Macdonald WL. 1970. Anatomical factors in resistance to Dutch elm disease. Netherlands Journal of Plant Pathology 76, 196-205.

Mensah JK, Sayer MAS, Nadel RL, Matusick G, Eckhardt LG. 2020. Physiological response of *Pinus taeda* L. trees to stem inoculation with *Leptographium terebrantis*. Trees 34, 869–880.

Mirone A, Brun E, Gouillart E, Tafforeau P, Kieffer J. 2014. The PyHST2 hybrid distributed code for high speed tomographic reconstruction with iterative reconstruction and a

priori knowledge capabilities. Nuclear Instruments and Methods in Physics Research Section B: Beam Interactions with Materials and Atoms 324, 41-48.

Morales-Cruz A, Allenbeck G, Figueroa-Balderas R, Ashworth VE, Lawrence DP, Travadon R, Smith RJ, Baumgartner K, Rolshausen PE, Cantu D. 2018. Closed-reference metatranscriptomics enables *in planta* profiling of putative virulence activities in the grapevine trunk disease complex: Transcriptomics of pathogen communities. Molecular Plant Pathology 19, 490-503.

Mugnai L, Graniti A, Surico G. 1999. Esca (Black Measles) and Brown Wood-Streaking : Two Old and Elusive Diseases of Grapevines. Plant Disease 83, 404-418.

Ouadi L, Bruez E, Bastien S, Vallance J, Lecomte P, Domec J-C, Rey P. 2019. Ecophysiological impacts of Esca, a devastating grapevine trunk disease, on *Vitis vinifera* L. PloS one 14, 1-20.

Ouellette GB, Baayen RP, Simard M, Rioux D. 1999. Ultrastructural and cytochemical study of colonization of xylem vessel elements of susceptible and resistant *Dianthus caryophyllus* by *Fusarium oxysporum* f.sp. Dianthi. Canadian Journal of Botany 77, 644-663.

Paganin D, Mayo SC, Gureyev TE, Miller PR, Wilkins SW. 2002. Simultaneous phase and amplitude extraction from a single defocused image of a homogeneous object. Journal of Microscopy 206, 33-40.

Pandey S, Rishi RR, Jayaraj R, Giri K, Kumar R, Pandey A, Juwantha R, Madaan S, Bhandari MS. 2019. *Fusarium equiseti* is associated with the wilt and dieback of *Aquilaria malaccensis* in Northeast India. Forest Pathology 49, e12489.

Park J-H, Juzwik J. 2014. *Ceratocystis smalleyi* colonization of bitternut hickory and host responses in the xylem. Forest Pathology 44, 282-292.

Parke JL, Oh E, Voelker S, Hansen EM, Buckles G, Lachenbruch B. 2007. *Phytophthora ramorum* Colonizes Tanoak Xylem and Is Associated with Reduced Stem Water Transport. Phytopathology 97, 1558-1567.

Pearce RB. 1996. Antimicrobial defences in the wood of living trees. New Phytologist 132, 203-233.

Pérez-Donoso AG, Lenhof JJ, Pinney K, Labavitch JM. 2016. Vessel embolism and tyloses in early stages of Pierce's disease. Australian Journal of Grape and Wine Research 22, 81-86.

Pita P, Rodríguez-Calcerrada J, Medel D, Gil L. 2018. Further insights into the components of resistance to *Ophiostoma novo-ulmi* in *Ulmus minor* : Hydraulic conductance, stomatal sensitivity and bark dehydration. Tree Physiology 38, 252-262.

Pouzoulet J, Mailhac N, Couderc C, Besson X, Daydé J, Lummerzheim M, Jacques A. 2013. A method to detect and quantify *Phaeomoniella chlamydospora* and *Phaeoacremonium aleophilum* DNA in grapevine-wood samples. Applied Microbiology and Biotechnology 97, 10163-10175.

Pouzoulet J, Scudiero E, Schiavon M, Rolshausen PE. 2017. Xylem Vessel Diameter Affects the Compartmentalization of the Vascular Pathogen *Phaeomoniella chlamydospora* in Grapevine. Frontiers in Plant Science 8, 1-13.

Pouzoulet J, Scudiero E, Schiavon M, Santiago LS, Rolshausen PE. 2019. Modeling of xylem vessel occlusion in grapevine. Tree Physiology 39, 1438-1445.

Pouzoulet J, Rolshausen PE, Charbois R, Chen J, Guillaumie S, Ollat N, Gambetta GA, Delmas CEL. 2020. Behind the Curtain of the Compartmentalization Process : Exploring How Xylem Vessel Diameter Impacts Vascular Pathogen Resistance. Plant, Cell & Environment doi: 10.1111/pce.13848.

Pratt RB, Jacobsen AL. 2018. Identifying which conduits are moving water in woody plants: A new HRCT-based method. Tree Physiology 38, 1200-1212.

Rioux D, Blais M, Nadeau-Thibodeau N, Lagacé M, DesRochers P, Klimaszewska K, Bernier L. 2018. First Extensive Microscopic Study of Butternut Defense Mechanisms Following Inoculation with the Canker Pathogen *Ophiognomonia clavigignenti-juglandacearum* Reveals Compartmentalization of Tissue Damage. Phytopathology 108, 1237-1252.

Salle A, Ye H, Yart A, Lieutier F. 2008. Seasonal water stress and the resistance of *Pinus yunnanensis* to a bark-beetle-associated fungus. Tree Physiology 28, 679-687.

Salleo S, Nardini A, Lo Gullo MA, Ghirardelli LA. 2002. Changes in stem and leaf hydraulics preceding leaf shedding in *Castanea sativa* L. Biologia plantarum 45, 227-234.

Schneider CA, Rasband WS, Eliceiri KW. 2012. NIH Image to ImageJ : 25 years of image analysis. Nature Methods 9, 671-675.

Shigo AL. 1984. Compartmentalization: A conceptual framework for understanding how trees grow and defend themselves. Annual Review of Phytopathology, 22, 189–214.

Sperry JS, Donnelly JR, Tyree MT. 1988. A method for measuring hydraulic conductivity and embolism in xylem. Plant, Cell & Environment 11, 35-40.

Solla A, Gil L. 2002. Xylem vessel diameter as a factor in resistance of *Ulmus minor* to *Ophiostoma novo-ulmi*. Forest Pathology 32, 123-134.

Sun Q, Rost TL, Matthews MA. 2008. Wound-induced vascular occlusions in *Vitis vinifera* (Vitaceae) : Tyloses in summer and gels in winter. American Journal of Botany 95, 1498-1505.

Sun Q, Sun Y, Walker MA, Labavitch JM. 2013. Vascular Occlusions in Grapevines with Pierce's Disease Make Disease Symptom Development Worse. Plant Physiology 161, 1529-1541.

Surico G, Marchi G, Ferrandino A, Braccini P, Mugnai L. 2000. Analysis of the spatial spread of esca in some Tuscan vineyards (Italy). Phytopathologia Mediterranea 39, 211-224.

Talboys PW. 1972. Resistance to Vascular Wilt Fungi. Proceedings of the Royal Society of London. Series B, Biological Science 181, 319-332.

Torres-Ruiz JM, Sperry JS, Fernández JE. 2012. Improving xylem hydraulic conductivity measurements by correcting the error caused by passive water uptake. Physiologia Plantarum 146, 129-135.

Travadon R, Lecomte P, Diarra B, Lawrence DP, Renault D, Ojeda H, Rey P, Baumgartner K. 2016. Grapevine pruning systems and cultivars influence the diversity of wood-colonizing fungi. Fungal Ecology 24 82-93.

Tyree MT, Sperry JS. 1989. Vulnerability of Xylem to Cavitation and Embolism. Annual Review of Plant Physiology and Plant Molecular Biology 40, 19-38.

Tyree MT, Ewers FW. 1991. The hydraulic architecture of trees and other woody plants. New Phytologist 119, 345-360.

Úrbez-Torres JR, Peduto F, Vossen PM, Krueger WH, Gubler WD. 2013. Olive Twig and Branch Dieback: Etiology, Incidence, and Distribution in California. Plant Disease 97, 231-244.

Venturas M, López R, Martín JA, Gascó A, Gil L. 2014. Heritability of *Ulmus minor* resistance to Dutch elm disease and its relationship to vessel size, but not to xylem vulnerability to drought. Plant Pathology 63, 500-509.

Yadeta KA, Thomma BPHJ. 2013. The xylem as battleground for plant hosts and vascular wilt pathogens. Frontiers in Plant Science 4 doi:10.3389/fpls.2013.00097.

Yazaki K, Takanashi T, Kanzaki N, Komatsu M, Levia DF, Kabeya D, Tobita H, Kitao M, Ishida A. 2018. Pine wilt disease causes cavitation around the resin canals and irrecoverable xylem conduit dysfunction. Journal of Experimental Botany 69, 589-602.

Zimmermann MH. 1979. The Discovery of Tylose Formation by a Viennese lady in 1845. IAWA Bulletin 2, 51-56.

TABLES

Table 1. Esca leaf symptom observations over the experimental season on *Vitis vinifera* cv Sauvignon blanc.

Symptom notation before 2019 / Symptom notation in 2019	All plants	Previously asymptomatic (pA)	Previously symptomatic (pS)
Esca-symptomatic	35 % (20/58)	30 % (6/20)	37 % (14/38)
Control-asymptomatic	65 % (38/58)	70 % (14/20)	63 % (24/38)

Plants are grouped by their symptom history: previously asymptomatic (pA, plants that have never expressed leaf symptoms between 2012 and 2018) and previously symptomatic (pS, plants that have expressed leaf symptoms at least once since 2012). Ratios present the number of plants in each symptom category (esca-symptomatic or control-asymptomatic) over the total number of plants of the category.

Table 2. Values for specific stem hydraulic conductivity (k_s), theoretical stem hydraulic conductivity (k_{th}) and equations of regression lines between k_s and k_{th} for control and esca symptomatic stems.

Tyloses	Esca	k_s [kg s^{-1} m^{-1} MPa^{-1}]	k_{th} [kg s^{-1} m^{-1} MPa^{-1}]	n (stem - plant)	Regression
Absence	Control	24.97 ± 1.72	78.36 ± 4.51	39 - 23	k_s = 0.3 x k_{th} + 1.6 R^2=0.61 P<0.0001
	Asymptomatic before symptoms	26.04 ± 4.71	74.75 ± 11.80	6 - 6	k_s = 0.36 x k_{th} - 0.94 R^2=0.82 P=0.013
	Pre-symptomatic	30.32 ± 4.26	87.88 ± 8.54	11 - 7	k_s = 0.37 x k_{th} - 1.9 R^2=0.54 P=0.010
	Asymptomatic after symptoms	19.80 ± 5.18	72.58 ± 12.64	5 - 2	k_s = 0.33 x k_{th} - 4 R^2=0.64 P=0.104
	Esca (tiger-stripe)	21.29 ± 5.40	72.85 ± 10.41	9 - 5	k_s = 0.45 x k_{th} - 11.26 R^2=0.74 P=0.003
Presence	Esca (tiger-stripe)	11.27 ± 2.86	70.44 ± 7.81	15 - 5	k_s = 0.17 x k_{th} -0.84 R^2=0.22 P=0.077
	Esca (apoplectic)	2.47 ± 1.45	74.80 ± 33.48	3 - 2	k_s = 0.04 x k_{th} - 0.2 R^2=0.68 P=0.385
Absence	All	25.06 ± 1.46	78.42 ± 3.37	70 - 37	k_s = 0.34 x k_{th} - 1.90 R^2=0.63 P<0.0001
Presence	All	9.81 ± 2.51	71.16 ± 8.00	18 - 7	k_s = 0.12 x k_{th} - 1.28 R^2=0.15 P=0.117

Values represent mean ± SE. n = sample size, (including the number of analyzed stems and-number of analyzed plants, respectively). See text and Fig. 4 for statistical analysis. A detailed esca symptom notation is provided in Fig. 1A. Bivariate plots of each regression are presented in Fig. S4.

Table 3. Long-term impact of symptom presence (i.e. comparing plants with different disease history record) in control plants on specific stem hydraulic conductivity (k_s), theoretical stem hydraulic conductivity (k_{th}), stem total vessel density, and amount of *Phaeomoniella chlamydospora* and *Phaeoacremonium minimum* DNA in trunks of plants without foliar symptoms.

	Previously asymptomatic (pA)	**Previously asymptomatic (pS)**	**Type III Tests of Fixed Effects (pA vs pS)**
k_s [kg s^{-1} m^{-1} MPa^{-1}]	23.76 ± 2.30	26.54 ± 2.61	n=39, $F_{1,16}$=1.19, P=0.29
k_{th} [kg s^{-1} m^{-1} MPa^{-1}]	72.22 ± 4.85	86.30 ± 7.98	n=39, $F_{1,16}$=3.01, P=0.10
total vessel density [count mm^{-2}]	57.28 ± 4.03	52.61 ± 3.25	n=39, $F_{1,16}$=0.72, P=0.41
P. chlamydospora [pg ng^{-1}]	6.14 ± 1.90	10.15 ± 3.41	**n=13, $F_{1,11}$=5900.06, P<0.0001**
P. minimum [pg ng^{-1}]	9.27 ± 6.97	26.40 ± 13.83	**n=13, $F_{1,11}$=51014, P<0.0001**

Values represent means ± SE. Pathogen quantification was estimated as: pg fungal DNA ng^{-1} total DNA. Statistical tests used are individual generalized linear mixed models to compare pA vs pS plants (fixed effect) with the individual plants entered as a random effect in the models and the year of uprooting as a co-variable (fixed effect). Statistically significant results (P<0.05) are shown in bold.

Table 4. Quantification by qPCR of *Phaeomoniella chlamydospora* and *Phaeoacremonium minimum* DNA in stems and trunks of different esca symptomatology.

Organ	Esca	n	*P. chlamydospora* [pg ng^{-1}]	*P. minimum* [pg ng^{-1}]
Stem	Control	8	0	0
	Pre-symptomatic	3	0	0
	Asymptomatic (after symptoms)	3	0	0
	Tiger-stripe (without tyloses)	4	0	0
	Tiger-stripe (with tyloses)	8	0	0
	Apoplectic	2	0	0
Trunk	Control	13	7.37 ± 1.67 (12/13)*	14.54 ± 6.51 (12/13)*
	Symptomatic	7	15.80 ± 3.12 (7/7)*	23.90 ± 8.82 (7/7)*

* Number of samples positive for the pathogen over the total number of analyzed samples.

Pathogen quantification was estimated as: pg fungal DNA per ng total DNA. Values represent means ± SE, n = sample size. Trunks of symptomatic plants presented higher amount of both *P. chlamydospora* and *P. minimum*, compared to control (n=20, $F_{1,18}$=29806.11.25, P<0.0001 and n=20, $F_{1,18}$=21925.4, P<0.0001, respectively). See text for statistical methods.

FIGURES

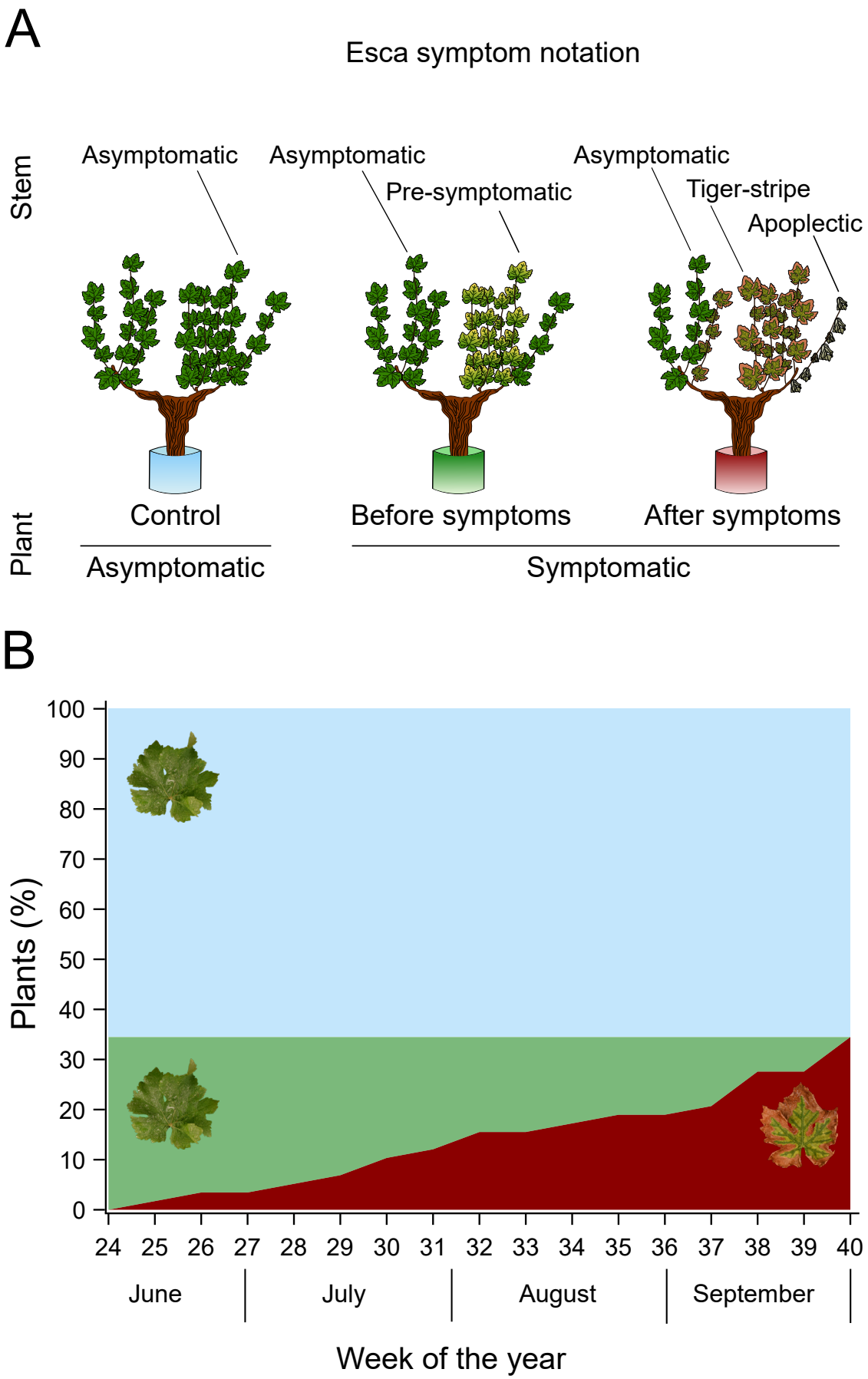

Fig. 1. Representation of esca symptom notation during the experimental season. (**A**) Single stems could be noted as esca asymptomatic, pre-symptomatic, tiger-stripe, or apoplectic. Whole plants have been noted as control (asymptomatic from June to October) or symptomatic (with tiger-stripe symptoms at the end of the season). (**B**) Proportion of plants in each symptom category over the experimental season (n=58). The blue area corresponds to control plants, green area to esca symptomatic plants before symptom appearance, and red area to esca symptomatic plants.

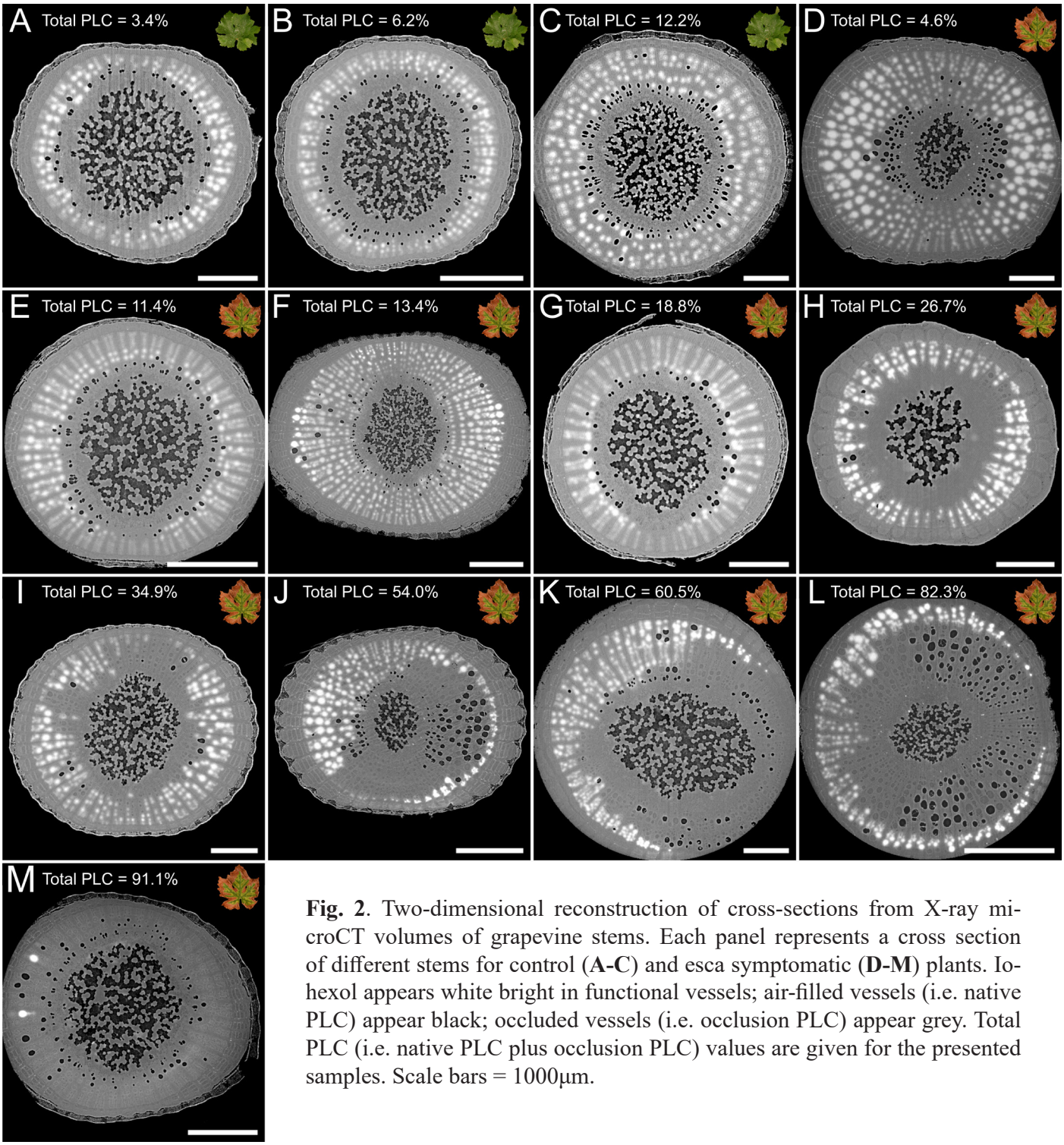

Fig. 2. Two-dimensional reconstruction of cross-sections from X-ray microCT volumes of grapevine stems. Each panel represents a cross section of different stems for control (**A-C**) and esca symptomatic (**D-M**) plants. Iohexol appears white bright in functional vessels; air-filled vessels (i.e. native PLC) appear black; occluded vessels (i.e. occlusion PLC) appear grey. Total PLC (i.e. native PLC plus occlusion PLC) values are given for the presented samples. Scale bars = 1000µm.

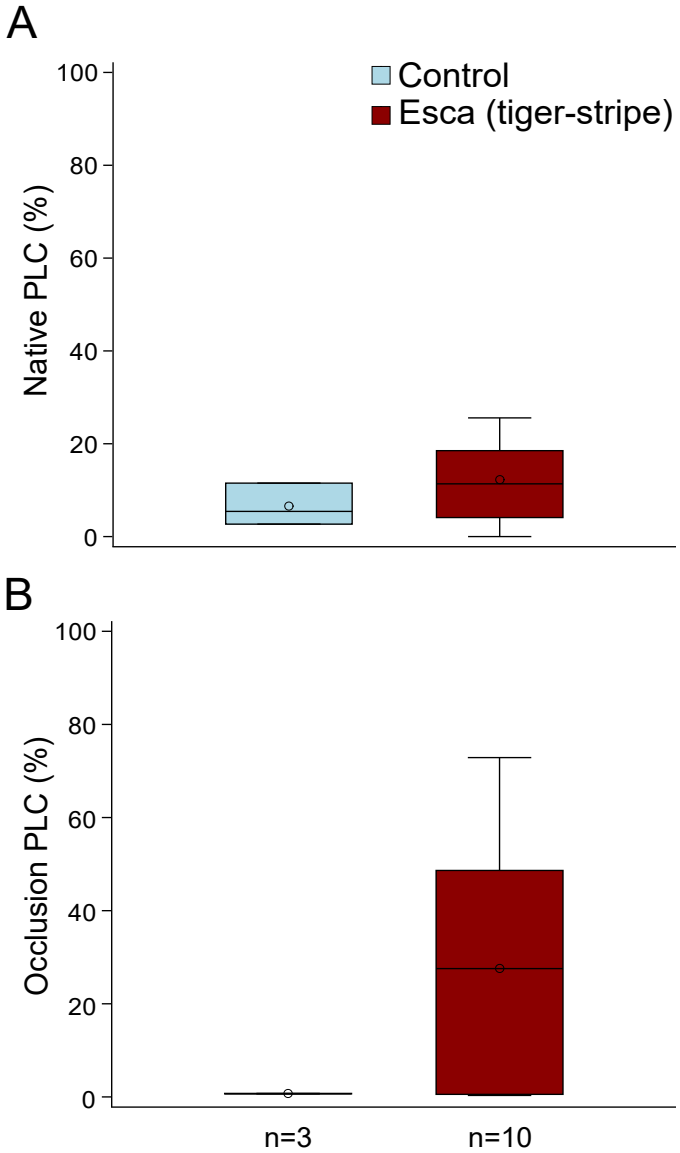

Fig. 3. (**A**) Mean values of native PLC in control (blue) and esca tiger-stripe (red) stems of grapevine plants using X-ray microCT imaging. Differences were not significant (n=13, $F_{1,9}$=0.07, P=0.79). (**B**) Mean values of occlusion PLC in control (blue) and esca tiger-stripe (red) stems of grapevine plants using X-ray microCT imaging. Differences were not significant (n=13, $F_{1,9}$=0.33, P=0.58). Boxes and bars show the median, quartiles and extreme values, circles show mean values. N represents the sample size (number of analyzed stems) for each group.

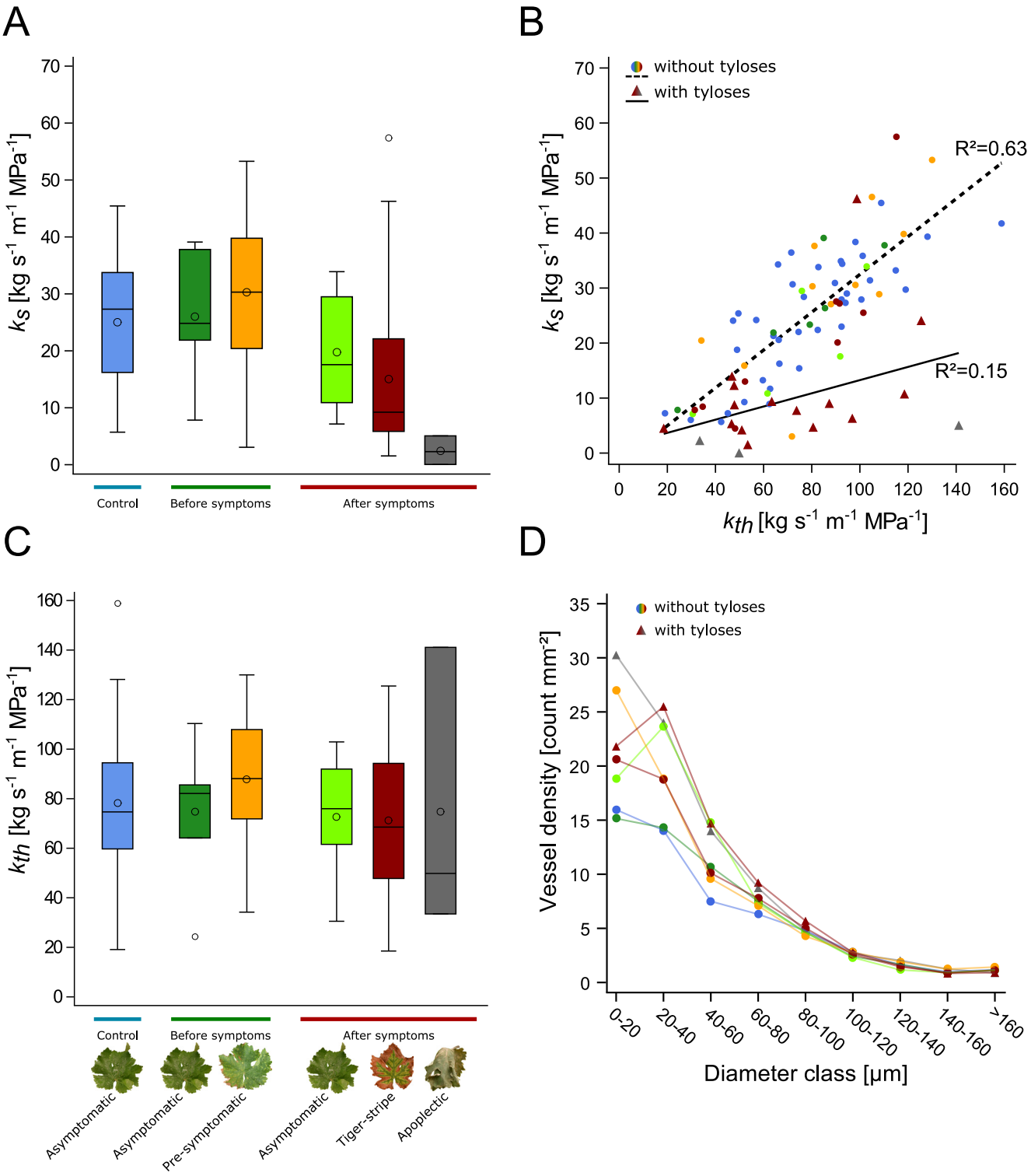

Fig. 4. Relationships between specific stem hydraulic conductivity (k_s), theoretical stem hydraulic conductivity (k_{th}), and vessel density in control and esca symptomatic grapevine plants. (**A**) k_s values for control (blue); asymptomatic (dark green) and pre-symptomatic (yellow) stems in plants before symptom appearance; asymptomatic (light green), tiger-stripe (red), and apoplectic (grey) stems in plants after symptom appearance, differences were not significant (n=88, $F_{5,45}$=1.30 P=0.28). Boxes and bars show the median, quartiles and extreme values, circles within boxes correspond to means, and circles outside boxes to outlier values. (**B**) Relationships between k_s and k_{th}. Symbols represent the absence (circles) or presence (triangles) of tyloses in xylem vessels. Colors represent esca symptomatology (as in panel A). The dashed line represents the regression for stems in which no tyloses were observed in xylem vessels, and the solid line represents the regression for samples with tyloses. R^2 for the regression lines are indicated (see Table 2 and Fig. S4 for detailed analyses). (**C**) k_{th} values for the different stem categories as presented in panel a. Differences were not significant (n=88, $F_{5,45}$=0.58, P=0.71). (**D**) Relationships between mean values of xylem vessel density and their diameters. Differences in total vessel density and in vessel size distributions were not significant (n=88, $F_{6,45}$=0.77, P=0.60; n=792 (88 samples for 9 vessel classes), $F_{48,693}$=1.19, P=0.18). Colors and markers are the same as panel B.